Exploring the Impact of Pure Copper Powder Reuse on Surface Chemistry During Powder Bed Fusion-Electron Beam

Surface and Interface Analysis

WILEY

SURFACE and INTERFACE ANALYSIS

RESEARCH ARTICLE OPEN ACCESS

Exploring the Impact of Pure Copper Powder Reuse on Surface Chemistry During Powder Bed Fusion-Electron Beam

Sofia Kazi[1] | Phillip Mahoney[2] | Eduard Hryha[1]

[1]Department of Industrial and Materials Science, Chalmers University of Technology, Gothenburg, Sweden | [2]Collibrium Additive, Arcam EBM, Gothenburg, Sweden

Correspondence: Sofia Kazi (sofiakaz@chalmers.se)

Received: 30 September 2024 | **Revised:** 20 August 2025 | **Accepted:** 1 September 2025

Funding: This work was supported by the Swedish Governmental Agency of Innovation Systems (Vinnova).

Keywords: additive manufacturing | oxidation | oxide layer thickness | powder | powder bed fusion–electron beam | pure copper | surface chemistry | X-ray photoelectron spectroscopy

ABSTRACT

The degradation of powder feedstock during additive manufacturing (AM) processes can significantly impact part quality, material utilization, and overall process sustainability. Pure copper, a material with high optical reflectivity, excellent thermal and electrical conductivity, is a promising candidate for powder bed fusion–electron beam (PBF-EB) manufacturing due to the process's ability to melt materials regardless of reflectivity under a controlled vacuum environment that prevents oxidation. This study examines the effects of pure copper powder properties and powder reuse on surface oxide chemistry and subsequent processability in PBF-EB. High-resolution scanning electron microscopy (HR-SEM) and X-ray photoelectron spectroscopy (XPS) were used to analyze changes in powder surface chemistry before and after reuse. The results demonstrate changes in surface chemistry with an elevated oxygen content, a thicker surface oxide layer, and the transformation of CuO to Cu_2O, as well as the formation of $Cu(OH)_2$ on the powder surface during handling. These changes can adversely affect the AM process, potentially leading to defects, reduced part quality, and decreased material utilization.

1 | Introduction

In recent years, metal manufacturing has been revolutionized with the emergence of additive manufacturing (AM). Initially developed as a small-scale prototyping step in the fabrication chain, AM has now developed into a transformative technology with its innovative approach of layer upon layer addition of material, a contrast to traditional metal subtractive technologies. Powder bed fusion (PBF) processes incorporate the consolidation of powder into components by fusing selected parts of the powder bed with the use of a focused energy source. In the case of PBF-EB, an electron beam provides the required energy to melt the powder and create complex geometries with high resolution.

Some of the main advantages of PBF-EB include the manufacturing of dense components at elevated temperatures with lower residual stresses [1]. The employment of the electron beam allows the processing of materials with higher melting points as opposed to PBF–laser beam (PBF-LB). PBF-EB utilizes a controlled vacuum environment within the printing chamber to optimize energy transfer. This vacuum creates a clear path for high-energy electrons to efficiently reach the target material, leading to optimal material melting. To prevent powder smoke-related issues, the spread layer is scanned before melting. Preheating of the powder bed is carried out, increasing its electrical conductivity and mitigating thermal shocks, which are particularly beneficial for crack-prone materials. A defocused electron beam is used to evenly distribute heat throughout the

build, ensuring consistent temperature control and preventing defects.

PBF processes offer the potential for sustainable manufacturing through powder recycling. However, the pre-sintering and long-term exposure to high temperatures during the build processes can introduce oxidation to the powder, particularly for oxidation-sensitive elements due to trace amounts of residual oxygen and humidity. This oxidation can lead to a higher oxygen content in the recycled powder compared with its original state. After the build, the powder forms a "sinter cake" that surrounds the printed parts. This "sinter cake" is typically removed using a blasting process that is carried out under atmospheric pressure using the build powder as abrasive media [2], which can also contribute to powder oxidation [3]. Studies have shown that PBF-EB processes, such as those used for TiAl6V4, can increase the oxidation rate of the powder compared to other methods like PBF-LB [4]. While powder recycling can enhance sustainability, it is essential to carefully consider the potential for oxidation and its impact on the properties of the printed components.

The unique conditions of PBF–electron beam (PBF-EB) processing, including vacuum and elevated temperatures, can lead to material degradation for certain alloys. Such long-term exposure can result in the formation of heterogeneous oxide layers on the powder particles [5], altering their surface chemistry and physical properties. For example, studies on alloy 718 have shown that plasma-atomized powder can develop coarse Al-based oxide particulates on the surface, which can grow in size and number with reuse [6]. In contrast, bulk 718 samples exhibit a more stable oxide composition, but with a lower oxygen level compared with the powder [7]. In addition, the sublimation of volatile elements, such as chromium (Cr) and aluminum (Al) in alloy 718, can take place during the PBF-EB process, leading to the loss of alloying elements [5]. The morphology and rheological behavior of Inconel 718 particles can also be affected by reuse. Previous research has suggested that blasting after printing can reduce satellite presence and deformation, while changes in surface oxide composition can alter the flow properties of the powder [8].

Pure copper is a popular choice for PBF-EB manufacturing due to its exceptional thermal and electrical conductivity. While copper has been used in PBF–laser beam (PBF-LB), its high reflectivity poses challenges for this technology [9]. PBF-LB is generally more suitable for materials with low reflectivity and thermal conductivity. Given that PBF-EB is unaffected by reflectivity, it offers a promising solution for producing complex, dense copper components. Characterization studies of pure copper powders intended for PBF-LB have revealed the presence of various copper oxides, including Cu_2O, CuO, and $Cu(OH)_2$ [10, 11], with their proportions varying based on particle size distribution (PSD). The finest powders tend to have the thinnest oxide layers [11]. The purity of the copper can also influence the growth of the oxide layer during AM [10]. Impurities in the copper can accelerate the oxidation process, leading to a thicker oxide layer with repeated reuse. The presence of trace elements as well as oxygen has also been shown to result in poorer electrical and thermal conductivity [12–14]. The oxygen content has also been proven to play a crucial role in the manufacturing of crack-free components, where printing of pure copper using powders with high oxygen content ~500 ppm resulted in samples with cracks at grain boundaries and weak mechanical properties, whereas the parts printed using powder containing low oxygen levels ~200 ppm demonstrated excellent mechanical performance and a microstructure free of cracks [15].

This study aims to explore the effects of PBF-EB processing on pure copper, focusing on both the powder's morphological characteristics and the changes in surface chemistry. High-resolution scanning electron microscopy (HR-SEM) and X-ray photoelectron spectroscopy (XPS) were employed to aid in the analysis of the surface oxides of the powder in both virgin and reused states and assessment of oxide layer thickness.

2 | Materials and Methodology

This study focused on oxygen-free high conductivity copper (OFH-Cu) powder produced by ECKART GmbH using inert gas atomization. The powder exhibited a PSD of $D_{10} = 50.5\,\mu m$, $D_{50} = 72\,\mu m$, and $D_{90} = 98.6\,\mu m$ as determined by laser diffraction (ISO 133320-10) and contained 195-ppm bulk oxygen.

The copper powder was processed using an ARCAM EBM Q10 metal PBF machine equipped with a Spectra EBU version 1.2. To prevent material evaporation during the electron beam melting process, the chamber was initially evacuated to a high vacuum before being filled with helium gas. Table 1 provides an overview of the powder samples analyzed. These included a virgin powder, as-received from the manufacturer and not exposed to the machine's conditions, and reused powders (×6 and ×8) recovered after printing and powder bed breakdown. Additionally, a variant of ×6 (×6/b) was processed under different conditions, using helium gas of lower purity. Sintered powder encapsulated in a printed enclosed component was also recovered from the powder bed. The purpose of the printed capsule was to keep the sintered powder isolated and curb the effects of handling and potential moisture.

The powder samples were gently pressed onto carbon tape to examine the surface morphology of the particles using HR-SEM. A Leo Gemini 450 SEM, Zeiss GmbH, equipped with a field-emission gun and in-lens detector was employed for this purpose. Imaging was conducted at an accelerating voltage of 10 kV and a working distance of 8.5 mm to characterize the particle surfaces.

To characterize the powder surface chemistry and characteristics of the surface oxide layer, XPS was employed using a PHI

TABLE 1 | The annotation of the samples based on the amount of print jobs in machine.

Sample name	No. of print jobs
Virgin	—
×6	6
×6/b	6
×8	8
Sintered	1

5000 (Physical Electronics, MN, USA) spectrometer equipped with a monochromatic Al Kα X-ray source (1486.6 eV). Survey and high-resolution narrow elemental scans were acquired using 14- and 26-eV pass energy, respectively, to determine elemental composition. Depth profiling was conducted using an Ar^+ ion gun sputtering to remove successive layers of material, enabling measurement of oxide layer thickness. A Ta_2O_5 standard plate was used to calibrate the etching rate, and hence, the oxide thickness reported in this study is equivalent to Ta_2O_5 units. Data analysis was performed using the PHI Multipak software.

3 | Results and Discussion

3.1 | Powder Morphology

Scanning electron microscopy (SEM) revealed the surface morphology of the powders, see Figure 1. The surface morphology of the powders varied across samples, indicating different effects of the printing cycles. Closer examination revealed a thin oxide layer with embedded coarse and flaky nanoparticles decorating the surface of the virgin, ×6 and ×powders. The ×6/b exhibited

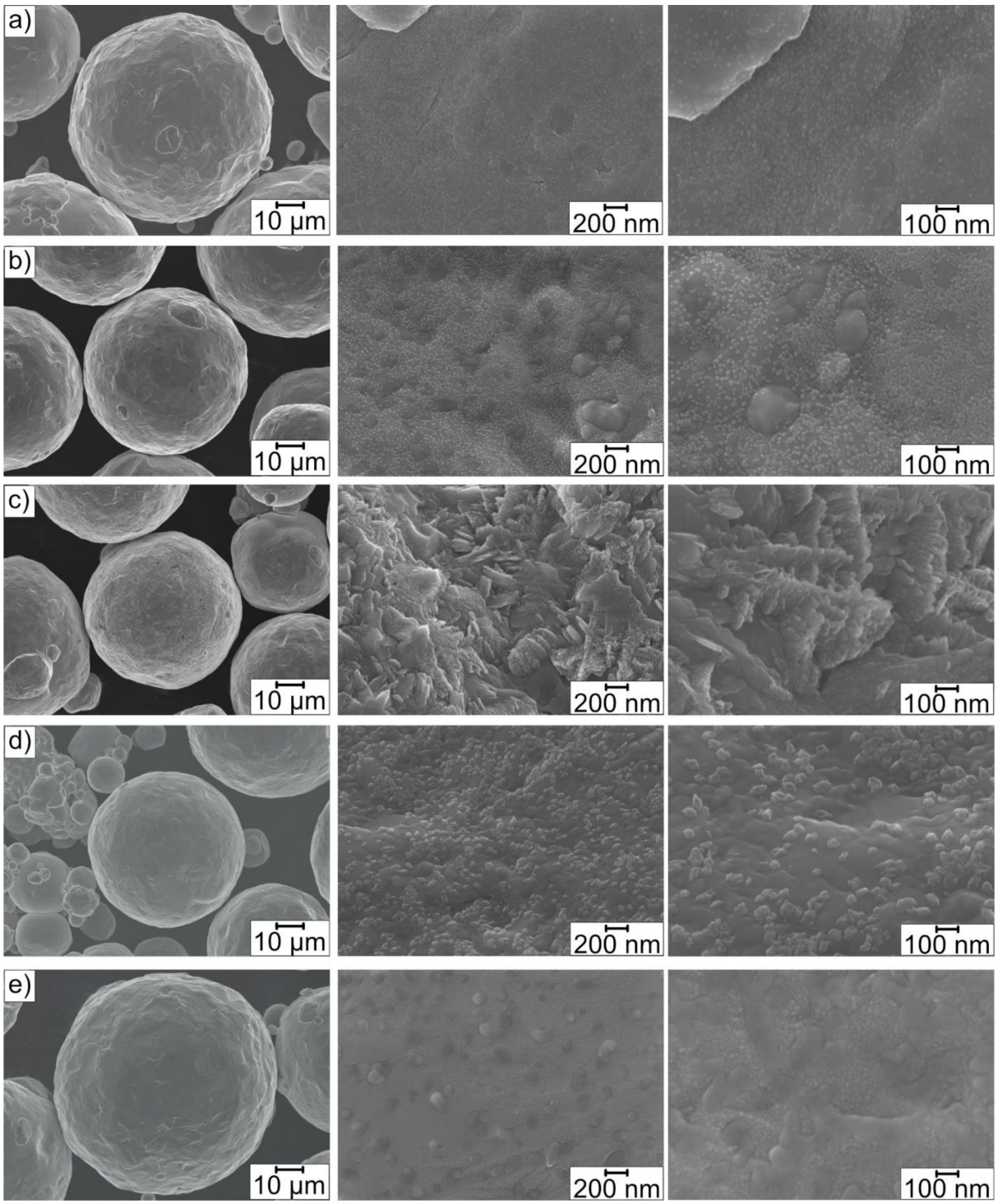

FIGURE 1 | SEM micrographs at low and high magnifications of the (a) virgin, (b) ×6, (c) ×6/b, (d) ×8, and (e) sintered powder.

coarse, nodule-like oxide scale while the sintered powder shows the presence of coarse dark islands.

3.2 | Powder Surface Analysis by XPS

In order to study the impact of the PBF-EB process on the copper powder properties and reusability, XPS high-resolution spectra of $Cu2p_{3/2}$ and O1s were recorded and analyzed as seen in Figure 2. Here, a shift correction in the binding scale was performed to alleviate the contamination of adventitious carbon originating from exposure to the atmosphere by placing the C1s peak at 284.8 eV. XPS analysis of pure powder standards of Cu_2O, CuO, and Cu $(OH)_2$ was performed as well to aid in the identification of chemical states in the copper samples, and the corresponding peak positions can be seen in Table 2.

With guidance of these reference peaks, the main $Cu2p_{3/2}$ peak for all samples was located at 932.6 eV (±0.01 eV). The peak position is indicative of the presence of Cu_2O and/or Cu^0. Pure copper has two main oxides, Cu_2O and CuO. CuO has higher stability at low temperatures and high oxygen partial pressures and hence is more stable at room temperatures. Cu_2O has higher stability at higher temperatures and lower partial pressure of oxygen. Hence, partial reduction of CuO to Cu_2O with increased temperatures can be observed [16]. Broadening of the $Cu2p_{3/2}$ main peak is apparent in all samples, indicating presence of mixed oxides as well as Cu $(OH)_2$, a result of CuO binding with moisture at the-as received surface. The characteristic satellite peak recorded at 940–950 eV is observed in all samples and indicates the presence of CuO in all powders to some extent, whereas it is the main oxide in ×6/b powder, see Figure 3c.

Detailed peak fitting was performed on the $Cu2p_{3/2}$ and O1s spectra of all samples by employing the asymmetric Shirley function, as seen in Figure 3. Although the differentiation between Cu_2O and Cu^0 peaks proved difficult to achieve in the $Cu2p_{3/2}$ main peak, due to the small difference in binding energies that have been reported in the literature [17], peak fitting confirmed the simultaneous presence of both CuO and Cu_2O, alongside Cu $(OH)_2$. The Auger Cu $L_3M_{45}M_{45}$ peak was also recorded, as seen in Figure 2c, to aid in the identification of chemical states. The main peak, positioned at 916.7 eV (kinetic energy) as well as the shoulder for all samples except the ×6/b, is an indication of the presence of Cu_2O and Cu $(OH)_2$, while the shoulder at 918.4 eV that can also be distinguished in all but the ×6/b sample is an

TABLE 2 | XPS binding energies of pure standard powders.

Peak	Peak positions (±0.1 eV)
Cu^0	932.6 eV
Cu^{1+} (Cu_2O)	932.6 eV
Cu^{2+} (CuO)	933.9 eV
Cu^{2+} ($Cu(OH)_2$)	934.8 eV
O^{2-} (Cu_2O)	530.7 eV
O^{2-} (CuO)	529.7 eV
O^{2-} ($Cu(OH)_2$)	531.8 eV

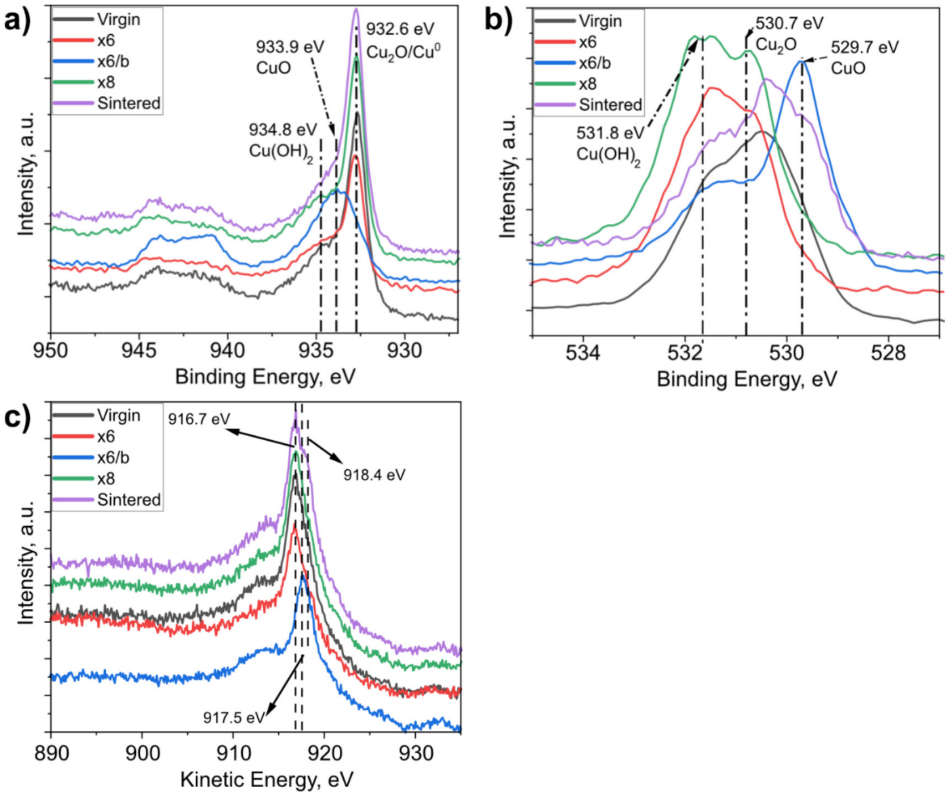

FIGURE 2 | XPS high-resolution spectra of the as-received surfaces capturing (a) the $Cu2p_{3/2}$ and the shake-up satellite region, (b) the O1s region and (c) the Cu $L_3M_{45}M_{45}$ region for all samples.

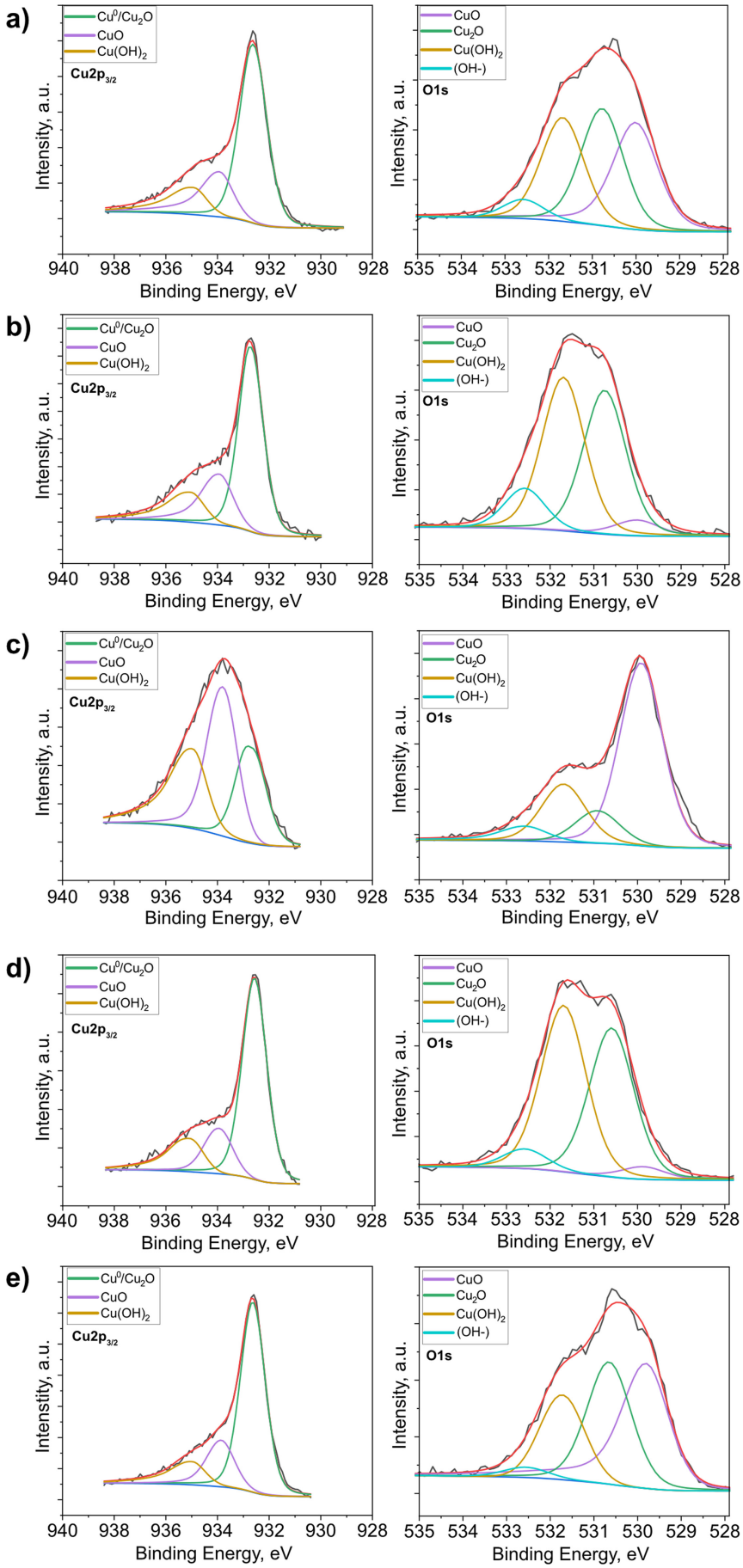

FIGURE 3 | XPS high-resolution narrow spectra of $Cu2p_{3/2}$ and O1s for (a) virgin, (b) ×6, (c) ×6/b, (d) ×8, and sintered powder.

indication of metallic Cu presence [10, 11]. The O1s spectra show a clear picture of the dominant oxide in each sample. For the virgin sample, as well as for ×6/b, the main oxide is CuO, and for ×6 and ×8 samples, the main oxide becomes Cu_2O. This change in chemical state can be attributed to the processing in PBF-EB under high vacuum at elevated temperatures, resulting in oxide transformation to Cu_2O as well as the post-processing procedure of exposing the samples to air and blasting it to break the sinter cake.

The samples that underwent different processing showcased a different trend. The ×6/b and sintered powders retained CuO as the main oxide on the surface. Then ×6/b was processed with a lower purity helium gas, and the sintered powder was contained in a printed lattice structure to minimize the effects of exposure to air after printing. The introduction of lower purity helium during the printing process leads to an increase in oxygen partial pressure during PBF-EB processing and hence leads to higher stability of CuO[16]. In the case of the sintered powder sample, it is assumed that a higher fraction of Cu_2O is present, also in agreement with SEM observation in Figure 2, as well as the position of the Cu $L_3M_{45}M_{45}$ peak as seen in Figure 2c, whereas the fraction of CuO and Cu $(OH)_2$ is similar to virgin powder, as the sample had minimal exposure to the air, comparable with the virgin powder (no blasting operation was performed).

The concentration of Cu $(OH)_2$ also changes with reuse. The main oxide changes with reuse from CuO in the virgin to Cu_2O in ×6 and ×8. Controlled vacuum and elevated temperatures are responsible for the rise in Cu_2O and post-handling in air is responsible for the increase in CuO and Cu $(OH)_2$. However, in ×6/b sample, a decrease in the Cu $(OH)_2$ content can be observed after detailed peak fitting; see Figure 3c. This is believed to be connected to the lower exposure to the air and humidity rather than connected to PBF-EB processing. Because Cu $(OH)_2$ is a metastable phase, it decomposes to the more stable CuO at relatively low temperatures (~423 K) through a step called dehydration [18]. This reaction is further reinforced by vacuum and hence removal of desorbed humidity.

The intensity of the O1s peak is plotted in Figure 4 as a function of etch depth and is presented in Ta_2O_5, calibrated with Ta_2O_5 foil of known thickness. Oxygen fraction in virgin and ×6 powders showcases a significant drop in intensity in the 5 nm of etching the surface of samples. The ×6/b powder exhibits the broadest profile of the oxygen peak, indicating a thicker oxide layer and/or presence of fine oxide features on the powder surface. The sintered and ×8 samples, while exhibiting the same initial decrease in oxygen content as virgin and ×6, have more prominent shoulders before oxygen is removed completely from the samples' surfaces at around 40 nm. The presence of said shoulders, particularly in the sintered powder, is an indication of the presence of oxide particulates on the surface in addition to the thin homogeneous oxide layer. The oxide layer thickness was calculated as the average of the maximum and minimum intensity values $(I_O{}^{max}—I_O{}^{min})/2$ as a metric of the oxide/metal interface [10, 11]. The calculated oxide layer thicknesses are shown in Table 3. Overall, it can be concluded that in the case of the PBF-EB process, which is conducted under vacuum and high purity He gas, the oxidation of pure copper powder is low with

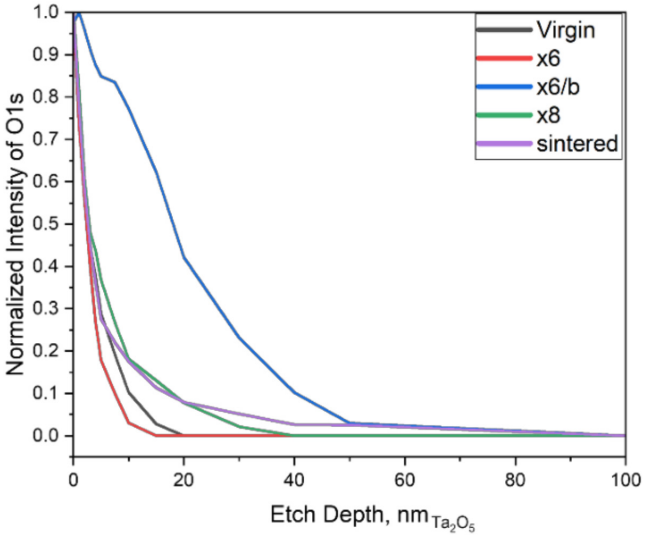

FIGURE 4 | Normalized intensity of O1s plotted against etch depth from XPS depth profiling.

TABLE 3 | Apparent oxide thickness derived from O1s normalized intensities in Figure 3.

Powder	Oxide layer thickness (nm)
Virgin	2.5
×6	2.4
×6/b	18.0
×8	2.8
Sintered	2.8

reuse, leading to potential for excellent reusability. The virgin powder showcased slightly higher oxide layer thickness than the ×6 variant, which is connected to the partial oxide layer removal during PBF-EB processing in the case of oxides with low thermodynamic stability [5–7, 16]. The ×6 and ×8 powders showcase a slow progressive increase in oxide layer thickness, as expected from reuse. The ×6/b was recovered from the printing process with the addition of the lower purity He, exhibiting the highest oxide layer thickness of 18 nm, which is in agreement with the SEM analysis of the powder where the nodule-like oxides covering the entire surface of the particles were observed. It is believed that the lower purity He gas was responsible for this fast degradation due to oxygen uptake.

Although universally agreed-upon industry thresholds for surface oxide layer thickness in pure copper powders for PBF-EB are not yet established, literature indicates that high oxygen contents and thick oxide scale formation are detrimental to the material properties of additively manufactured parts. Our study focused on surface oxide chemistry and found that, under controlled PBF-EB conditions, oxide layer growth is minimal over several reprocessing cycles. The oxide layer thickness in the samples increased only slightly (from 2.4 to 2.8 nm) implying that several reuse cycles are feasible before reaching critical thresholds in the case of well-controlled PBF-EB processing and proper powder handling with minimal exposure to the ambient

air and humidity. However, precise limits for oxide layer thickness or composition that would compromise the material properties, such as electrical and thermal conductivity, remain to be established in future work directly correlating oxide properties to part quality. In industrial settings, powder reuse protocols often include blending used powders with virgin batches to further extend powder life. Implementing constant exposure time during printing and reusing the same powder batch without mixing will be essential to study the powder's surface oxide layer thickness limits before disqualification.

4 | Conclusions

To examine the effects of PBF-EB processing on pure oxygen-free high-conductivity copper (OFHC-Cu) powder, both virgin and reused after PBF-EB processing powders were analyzed using XPS and SEM. SEM observations revealed distinct morphological variations in the oxide layers formed on the powder surfaces, suggesting changes in oxide composition with reuse under different conditions. XPS analysis confirmed that both powder reuse and exposure to PBF-EB processing conditions led to a transformation of the dominant oxide from a thin oxide layer primarily consisting of CuO, with the presence of Cu_2O and $(Cu(OH)_2)$ to a thin oxide layer that is formed during powder exposure to the air during post-AM processing/blasting with Cu_2O particulate oxide features, size and fraction of which are increasing with powder reuse. The thickness of the oxide layer was found to slightly increase with powder reuse and was found to provide a good indication of the process conditions during PBF-EB processing. Powder handling has a strong effect on powder surface oxide composition in the case of copper powders, with an increase in the fraction of Cu_2O and copper hydroxide $(Cu(OH)_2)$ with exposure to ambient conditions during powder handling and post-AM processing. Hence, it can be concluded that copper powder is very sensitive to handling and PBF-EB processing but possesses excellent reusability when properly handled and processed in a controlled environment.

Acknowledgements

This work was performed in the framework of the Centre for Additive Manufacturing—Metal (CAM^2), supported by the Swedish Governmental Agency for Innovation Systems (Vinnova).

Data Availability Statement

Data openly available in a public repository that issues datasets with DOIs.

References

1. L. M. Sochalski-Kolbus, E. A. Payzant, P. A. Cornwell, et al., "Comparison of Residual Stresses in Inconel 718 Simple Parts Made by Electron Beam Melting and Direct Laser Metal Sintering," *Metallurgical and Materials Transactions A, Physical Metallurgy and Materials Science* 46, no. 3 (2015): 1419–1432, https://doi.org/10.1007/S11661-014-2722-2.

2. W. Hung, "Postprocessing of Additively Manufactured Metal Parts," *Journal of Materials Engineering and Performance* 30 (2021): 6439–6460, https://doi.org/10.1007/s11665-021-06037-z.

3. G. Shanbhag and M. Vlasea, "Powder Reuse Cycles in Electron Beam Powder Bed Fusion—Variation of Powder Characteristics," *Materials* 14, no. 16 (2021): 4602, https://doi.org/10.3390/MA14164602.

4. N. Derimow and N. Hrabe, "Oxidation in Reused Powder Bed Fusion Additive Manufacturing Ti-6Al-4V Feedstock: A Brief Review," *JOM* 73 (2021): 3618–3638, https://doi.org/10.1007/s11837-021-04872-y.

5. A. Raza and E. Hryha, "Characterization of Spatter and Sublimation in Alloy 718 During Electron Beam Melting," *Materials* 14, no. 20 (2021): 5953, https://doi.org/10.3390/ma14205953.

6. H. Gruber, M. Henriksson, E. Hryha, and L. Nyborg, "Effect of Powder Recycling in Electron Beam Melting on the Surface Chemistry of Alloy 718 Powder," *Metallurgical and Materials Transactions A* 50 (2019): 4410–4422, https://doi.org/10.1007/s11661-019-05333-7.

7. H. Gruber, C. Luchian, E. Hryha, and L. Nyborg, "Effect of Powder Recycling on Defect Formation in Electron Beam Melted Alloy 718," *Metallurgical and Materials Transactions A* 51 (2020): 2430–2443, https://doi.org/10.1007/s11661-020-05674-8.

8. L. Cordova Gonzalez, A. Raza, and E. Hryha, "Rheological Behavior of Inconel 718 Powder for Electron-Beam Melting," *Metals* 12, no. 7 (2022): 1231, https://doi.org/10.3390/met12071231.

9. Q. Jiang, P. Zhang, Z. Yu, et al., "A Review on Additive Manufacturing of Pure Copper," *Coatings* 11, no. 6 (2021): 740, https://doi.org/10.3390/COATINGS11060740.

10. E. Bojestig, Y. Cao, and L. Nyborg, "Surface Chemical Analysis of Copper Powder Used in Additive Manufacturing," *Surface and Interface Analysis* 52 (2020): 1104–1110, https://doi.org/10.1002/sia.6833.

11. L. Nyborg and Y. Cao, "Surface Chemical and Geometrical Properties of Pure Copper Powder Intended for Binder Jetting and Sintering," *Surface and Interface Analysis* 54, no. 9 (2022): 944–953, https://doi.org/10.1002/sia.7107.

12. R. Guschlbauer, S. Momeni, F. Osmanlic, and C. Körner, "Process Development of 99.95% Pure Copper Processed via Selective Electron Beam Melting and Its Mechanical and Physical Properties," *Materials Characterization* 143 (2018): 163–170, https://doi.org/10.1016/J.MATCHAR.2018.04.009.

13. S. J. Raab, R. Guschlbauer, M. A. Lodes, and C. Körner, "Thermal and Electrical Conductivity of 99.9% Pure Copper Processed via Selective Electron Beam Melting," *Advanced Engineering Materials* 18 (2016): 1661–1666, https://doi.org/10.1002/adem.201600078.

14. Y. T. Hsu and B. O'reilly, "Impurity Effects in High-Conductivity Copper a Compilation of Second-Element Effects Showing That Marked Property Changes Can Be Noticed at Surprisingly Low Concentrations".

15. R. Guschlbauer, A. K. Burkhardt, Z. Fu, and C. Körner, "Effect of the Oxygen Content of Pure Copper Powder on Selective Electron Beam Melting," *Materials Science and Engineering A* 779 (2020): 139106, https://doi.org/10.1016/J.MSEA.2020.139106.

16. E. Hryha, E. Dudrova, and L. Nyborg, "On-Line Control of Processing Atmospheres for Proper Sintering of Oxidation-Sensitive PM Steels," *Journal of Materials Processing Technology* 212, no. 4 (2012): 977–987, https://doi.org/10.1016/J.JMATPROTEC.2011.12.008.

17. M. C. Biesinger, L. W. M. Lau, A. R. Gerson, and R. S. C. Smart, "Resolving Surface Chemical States in XPS Analysis of First Row Transition Metals, Oxides and Hydroxides: Sc, Ti, V, Cu and Zn," *Applied Surface Science* 257, no. 3 (2010): 887–898, https://doi.org/10.1016/J.APSUSC.2010.07.086.

18. Y. Cudennec and A. Lecerf, "The Transformation of Cu $(OH)_2$ Into CuO, Revisited," *Solid State Sciences* 5, no. 11–12 (2003): 1471–1474, https://doi.org/10.1016/J.SOLIDSTATESCIENCES.2003.09.009.